Cerebral Cortex, March 2017;27:2095–2110

doi:10.1093/cercor/bhw065
Advance Access Publication Date: 10 March 2016
Original Article

ORIGINAL ARTICLE

The Right Dorsal Premotor Mosaic: Organization, Functions, and Connectivity

Sarah Genon[1,2], Hai Li[5,6], Lingzhong Fan[5,6], Veronika I. Müller[1,2], Edna C. Cieslik[1,2], Felix Hoffstaedter[1], Andrew T. Reid[1], Robert Langner[1,2], Christian Grefkes[1,4], Peter T. Fox[3], Susanne Moebus[8], Svenja Caspers[1], Katrin Amunts[1], Tianzi Jiang[5,6,7] and Simon B. Eickhoff[1,2]

[1]Institute of Neuroscience and Medicine (INM-1, INM-3), Research Centre Jülich, Jülich, Germany, [2]Institute of Clinical Neuroscience and Medical Psychology, Heinrich Heine University, Düsseldorf, Germany, [3]Research Imaging Institute, University of Texas Health Science Center at San Antonio, TX, USA, [4]Department of Neurology, Cologne University Hospital, Cologne, Germany, [5]Brainnetome Center, Institute of Automation and, [6]National Laboratory of Pattern Recognition, Institute of Automation, Chinese Academy of Sciences, Beijing 100190, China, [7]Key Laboratory for NeuroInformation of the Ministry of Education, School of Life Science and Technology, University of Electronic Science and Technology of China, Chengdu 625014, China and [8]Centre for Urban Epidemiology (CUE), Universitätsklinikum Essen, University of Duisburg-Essen, Essen, Germany

Address correspondence to Simon B. Eickhoff, Institut für Neurowissenschaften und Medizin (INM-1), Forschungszentrum Jülich GmbH, D-52425 Jülich, Germany. Email: s.eickhoff@fz-juelich.de

Abstract

The right dorsal premotor cortex (PMd) of humans has been reported to be involved in a broad range of motor and cognitive functions. We explored the basis of this behavioral heterogeneity by performing a connectivity-based parcellation using meta-analytic approach applied to PMd coactivations. We compared our connectivity-based parcellation results with parcellations obtained through resting-state functional connectivity and probabilistic diffusion tractography. Functional connectivity profiles and behavioral decoding of the resulting PMd subregions allowed characterizing their respective behavior profile. These procedures divided the right PMd into 5 distinct subregions that formed a cognitive-motor gradient along a rostro-caudal axis. In particular, we found 1) a rostral subregion functionally connected with prefrontal cortex, which likely supports high-level cognitive processes, such as working memory, 2) a central subregion showing a mixed behavioral profile and functional connectivity to parietal regions of the dorsal attention network, and 3) a caudal subregion closely integrated with the motor system. Additionally, we found 4) a dorsal subregion, preferentially related to hand movements and connected to both cognitive and motor regions, and 5) a ventral subregion, whose functional profile fits the concept of an eye movement-related field. In conclusion, right PMd may be considered as a functional mosaic formed by 5 subregions.

Key words: activation likelihood estimation, clustering, functional connectivity, parcellation, premotor cortex

Introduction

The premotor cortex (PM) has been defined as a distinct cortical region within the frontal agranular cortex (Wise 1985). The PM is located in the lateral portion of Brodmann's area 6 (BA; Brodmann 1909) on the precentral gyrus, just rostral to the primary motor cortex (M1, BA 4/Area 4; Geyer et al. 2000).

However, the PM is not necessarily equivalent to BA 6, since the region defined as the PM is based on functional criteria, whereas BA 6 is identified by cytoarchitectonic criteria (Brodmann 1909; Geyer et al. 2000). In nonhuman primates, the PM has been anatomically subdivided into a dorsal part (PMd) and a ventral part (PMv) (for a review, see Rizzolatti et al. 1998). In primates, the PMd has been further divided into rostral and caudal subregions based on differences in connectivity (Abe and Hanakawa 2009) and histology (i.e., cytoarchitecture and cytochrome C staining). The rostral subregion, termed F7 (Matelli et al. 1985, 1991), is mainly connected to prefrontal regions, while the caudal subregion, termed F2 (Matelli et al 1991) is connected to the primary motor cortex and spinal cord (Boussaoud et al. 1995; Rizzolatti and Luppino 2001).

The dorso-ventral distinction in nonhuman primates shows correspondence with the subdivision of the human PM into PMd and PMv based on structural connectivity (Tomassini et al. 2007). A broad range of motor and cognitive functions, such as movement preparation, action selection, motor learning, goal salience maintenance, visuospatial imagery, visual attention, and working memory, have been ascribed to the PMd in humans (for reviews, see Boussaoud 2001; Schubotz and von Cramon 2003; Chouinard and Paus 2006; Hoshi and Tanji 2007; Abe and Hanakawa 2009; Kantak et al. 2012; Hoshi 2013). In conjunction with previously identified PMd subregions in nonhuman primates (i.e., F2, F7), such behavioral heterogeneity suggests that the human PMd may not be a uniform region, but rather one comprised several distinct subdivisions with specialized function and connectivity.

Several studies have suggested a rostro-caudal organization corresponding to a cognitive-motor gradient within the frontal regions including the PMd (Yeo et al. 2011; Choi et al. 2012; Orban et al. 2014). Furthermore, several fMRI experiments have been performed to disentangle PMd activity related to cognitive versus motor processing, or hand versus eye movements by contrasting experimental conditions in rather small samples of subjects (Hanakawa et al. 2002; Amiez et al. 2006). Finally, one study has suggested a ventrodorsal organization within the superior part of precentral gyrus based on structural connectivity (Schubotz et al. 2010). However, neither these putative anatomical gradients nor their corresponding behavioural and functional attributes have been directly investigated in the PMd, and by using a quantitative data-driven approach. Furthermore, to date, no study has examined the connectivity profile of distinct modules within the PMd in humans at rest or challenged with a wide range of task demands.

Using a model-free, multimodal, connectivity-based approach, we sought in the current study to provide a robust, data-driven subdivision of the right PMd, as well as a meta-analytic functional characterization of the resulting subdivisions. Our work may thus provide independent support for the idea of a rostro-caudal organization of the PMd, with rostral parts more strongly associated with cognitive functions, and caudal regions with motor functions and/or for the hypothesis of a ventrodorsal distinction. Our objective was to integrate previous work and hypotheses on the PMd. To best incorporate the findings of previous research lines, we opted for a broad definition of the right PMd, ensuring a maximal coverage of previous activations attributed to this region. Importantly, the issue of the functional heterogeneity of the PMd is further complicated by indirect evidence of functional hemispheric differences (Smith and Jonides 1999; Schubotz and von Cramon 2003), which might be based on differential subdivisions within the right and left PMd. Therefore, in the present study, we focused on the right PMd, while the organization of the left PMd will be addressed in a future study.

We performed connectivity-based parcellation (CBP) based on each voxel's co-activation pattern across a wide range of active tasks (MACM-CBP; Eickhoff et al. 2011). Our objective was not so much to define a rigid set of borders for subregions within the right PMd, but rather to provide an integrative guide of the topographical organization of this region. Accordingly, to ensure that the resulting general topographical pattern was not an artifact of the CBP modality, we performed additional CBP analyses based on the structural connectivity profile of the voxels, as measured by probabilistic diffusion tractography (PDT-CBP; Behrens et al. 2003; Johansen-Berg et al. 2004), and the functional connectivity profile, as measured during the resting state fMRI (RSFC-CBP). We next characterized the functional connectivity profile of the clusters obtained by MACM-CBP by combining resting-state functional connectivity (RSFC) analysis and MACM. Finally, quantitative functional decoding (Amft et al. 2015; Nickl-Jockschat et al. 2015) was performed to robustly characterize the profile of behavioral functions associated with each cluster obtained by MACM-CBP.

Methods

Volume of Interest

In the absence of precise landmarks of the borders of PMd, we based our volume of interest (VOI) definition on several meta-analyses that localized functions commonly attributed to the PMd. Our VOI was defined by merging PMd activation sites from published meta-analyses on action observation (Caspers et al. 2010), motor learning (Hardwick et al. 2013), movement perception (Grosbras et al. 2012), sustained attention (Langner and Eickhoff 2013), and working memory (Rottschy et al. 2012) using an or combination. The ensuing VOI was symmetrized to yield left and right PMd VOIs. Some activation clusters provided by the meta-analyses to some extend overlapped with primary motor cortex (M1) and primary somatosensory cortex (S1). These areas were excluded based on their cytoarchitectonic definition (Areas 4a, 4p 3a, 3b, 1, 2) by using the SPM Anatomy Toolbox (Eickhoff et al. 2005). Thus, this procedure ensures that our VOI does not overlap with primary motor cortex on the caudal border as illustrated in Figure 1. In contrast and importantly, our VOI was not restricted to Area 6 on the rostral border.

Finally, white matter voxels were removed from the VOI based on the International Consortium on Brain Mapping (ICBM) tissue probability maps (Mazziotta et al. 2001). This procedure yielded a

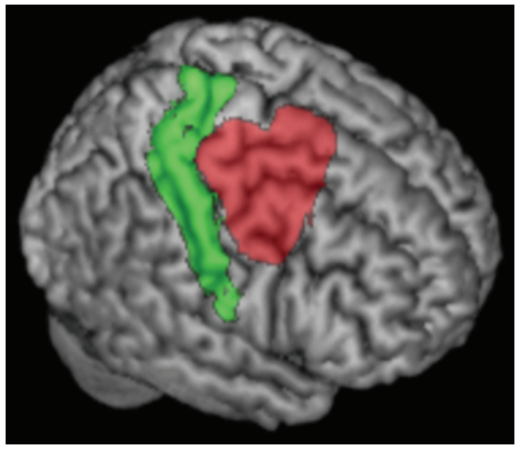

Figure 1. VOI definition. Rendering of sensorimotor areas (areas 1, 2, 3, and 4; green) according to cytoarchitecture (Geyer et al. 1996, 1999, available in the SPM anatomy toolbox) and our PMd VOI (red) in the right hemisphere.

right and a left PMd VOI, comprising 4143 voxels each (voxels size = 1 × 1 × 1) whose inferior and caudal borders are in agreement with previous definition of the PMd (see Supplementary Methods I.1.). The following parcellation procedure was focused on the right PMd VOI.

Connectivity-Based Parcellation

We first performed CBP based on the co-activation profiles of our VOI's voxels by using MACM. The most stable cluster solution (k solution) was chosen based on several criteria in a data-driven approach. To ensure that the revealed topographical organization was not an artifact of our methods based on activation data (cf. discussion), we then searched for a similar k solution based on the structural connectivity profiles of the voxels by using CBP based on PDT (PDT-CBP) and based on the unconstrained functional connectivity profiles of the voxels by using CBP based on RSFC (RSFC-CBP).

Parcellation Based on Co-activation (MACM-CBP).

Meta-Analytic Connectivity Modeling. Whole-brain co-activation patterns for each voxel within the right PMd were determined by using the BrainMap database (see Supplementary Methods I.2. for a description of the criteria of inclusion of experiments). The experiments associated with each seed voxel were then defined by activation at, or in the immediate vicinity of, this particular voxel. This was performed by calculating the Euclidean distances between a given seed voxel and the individual foci of all experiments. Based on these distances, the extent of a spatial filter was systematically varied from including the closest 20 to 200 experiments in steps of 5. That is, we selected the 20, 25, 30, 35, . . . , 200 experiments reporting activation closest to a given seed voxel. Combining the different filter sizes allowed generating a highly robust co-activation map for every seed voxel independently of subjective choices about the number of associated experiments. This procedure, hence, provided a reliable basis for MACM-CBP, as shown in previous studies (Cieslik et al. 2013; Clos et al. 2013).

The brain-wide co-activation profile for each seed voxel given each of the 37 filter sizes was then computed by a meta-analysis over the associated experiments. This meta-analysis was performed using the revised ALE algorithm (Eickhoff et al. 2012; see Supplementary Methods I.3. for a description of the use of ALE for MACM). All resulting ALE scores were recorded. To take into account the complete brain-wide pattern of co-activation likelihood of each seed voxel, no height threshold was set at this point of analysis.

Connectivity-Based Parcellation Using Co-activation Patterns. The brain-wide co-activation profiles for all seed voxels were combined into a $N_S \times N_B$ connectivity matrix. N_S is the number of seed voxels (i.e., 4143 voxels) and N_B the number of target voxels in the reference brain volume at $4 \times 4 \times 4$ mm^3 resolution (26 459 gray matter voxels). Altogether, 37 individual connectivity matrices were computed, each representing the connectivity of the seed voxels for a given filter size.

K-MEANS CLUSTERING. In line with previous parcellation studies (Klein et al. 2007; Kelly et al. 2012; Clos et al. 2013), the parcellation was performed using *k*-means clustering (see Supplementary Methods I.4. for a description of *k*-means). In line with previous parcellation studies of multifunctional regions, we addressed a wide range of potential subdivisions (Kelly et al. 2010, 2012; Kahnt et al. 2012). That is, we searched for 2–11 different clustering solutions by making *k* ranging from 2 to 11, yielding 10 different clustering solutions within the right PMd (a 2-cluster solution, a 3-cluster solution, and so on, up to an 11-cluster solution). For each of the 370 (10 × 37) individual parcellations, the best solutions from 500 replications with a randomly placed initial centroid were computed.

SELECTION OF THE OPTIMAL RANGE. Like in a previous study (Clos et al. 2013), the optimal filter range was chosen based on the consistency of each voxel's cluster assignment across the different filter sizes. Those analyses are reported in Supplementary Methods I.5. In all subsequent steps, the analysis was restricted to the parcellations based on co-activations as estimated from the nearest 85 to 145 experiments.

DATA-DRIVEN SELECTION OF THE OPTIMAL CLUSTERING SOLUTION. In the next step, we determined the optimal clustering solution, that is, the parcellation that was most supported by the data. This choice was based on 3 criteria: 1) variation of information, 2) percentage of deviants, and 3) silhouette value. The full description of these criteria is provided in Supplementary Methods I.6. The above criteria identified a 5k solution as the most stable parcellation of the right PMd.

Parcellation Based on Probabilistic Diffusion Tractography (PDT-CBP).

Data Acquisition and Preprocessing. Diffusion weighted imaging (DWI) data of 20 healthy adults were acquired using a 3.0 T GE MR Scanner (see Wang et al. 2015 for a full description of the data sample and acquisition parameters). The data were preprocessed using FMRIB's Diffusion Toolbox (FSL 4.0; http://www.fmrib.ox.ac.uk/fsl). The T_1 images obtained in diffusion space were transformed to the ICBM-152 brain template while an inverse transformation was performed to transform the VOI masks of the right PMd into the diffusion space for each subject.

Diffusion probabilistic tractography was performed using the FSL package for each voxel in the PMd seed VOI to estimate the connectivity probability as described in Wang et al. (2015).

Cross-Correlation Matrix, Parcellation, and Maximum Probability Map of the k Solution. Cross-correlations (dimensions: number of seeds × number of seeds) between the connectivity patterns of all voxels in the PMd seed VOI were calculated. The cross-correlation matrix was then permutated using spectral clustering (not spectral reordering). An edge-weighted centroidal Voronoi tessellations method for automated clustering was applied to define 5 clusters as revealed as the most stable cluster solution for MACM-CBP. Then, the maximum probability maps were created for each *k* solution across all the subjects (see Wang et al. 2015 for a full description of the CBP pipeline).

Parcellation Based on RSFC (RSFC-CBP). *Data Acquisition and Preprocessing*. EPI resting state data from 124 healthy subjects (age range: 18–59, mean ± standard deviation: 39.5 ± 11.5, 66 males) were acquired as part of the 1000 brains study (Caspers et al. 2014). A description of acquisition parameters is provided in Supplementary Methods I.7. Functional image processing was performed using SPM8 (Wellcome Trust Centre for Neuroimaging, London, http://www.fil.ion.ucl.ac.uk/spm/software/spm8). Prior to further analyses, the first 4 scans were discarded. Then, preprocessing of the EPI images included affine registration and normalization to MNI space using unified segmentation approach. A more comprehensive description of this procedure is available in Supplementary Methods I.7.

Cross-Correlation Matrix, Parcellation, and Maximum Probability Map of the k Solution. The time series were computed for each voxels when removing potentially noisy variance (see Supplementary Methods I.7. for a description of the procedure). Linear (Pearson) correlations between the time series of each seed voxels (cluster) and all other gray matter voxels were computed and z-transform to quantify RSFC. The individual connectivity matrices of the seeds voxels with the whole-brain gray matter voxels were built. *k*-Means (with *k* ranging from 2 to 9) was then performed on the individual connectivity matrices. Finally, the maximum probability maps were created for each *k* solution across all the subjects.

Multimodal Functional Connectivity of the MACM-CBP-Derived Clusters

Following the parcellations of the seed region, we examined the functional connectivity profile of each cluster by performing additional MACM and RSFC analyses of the obtained clusters. While MACM provides the co-activation pattern of the clusters across a wide range of active tasks, RSFC provides the complementary, task-free measure of functional connectivity of these clusters (Eickhoff et al. 2011).

We first computed the whole-brain connectivity pattern of each cluster and then examined the commonalities among clusters as well as the differences between them. In other words, for each modality (MACM and RSFC), we statistically tested both the conjunction of all clusters and the contrasts between them.

Task-Related Functional Connectivity (MACM).

Main Effects. For each obtained PMd subregion, an ALE meta-analysis was performed across all BrainMap experiments featuring at least one focus of activation within each of the derived clusters using the same approach as described above. In contrast to the MACM underlying CBP, where ALE maps were not thresholded to retain the complete pattern of co-activation likelihoods, we now performed statistical inference by testing the observed ALE scores from the actual meta-analysis against ALE scores obtained under the null distribution of random association of foci between experiments. A full description of this procedure is provided in Supplementary Methods I.8. This test yielded a *P* value based on the proportion of equal or higher random values. The resulting non-parametric *P* values were transformed into z-scores and thresholded at a cluster level with family-wise error rate (FWE)-corrected $P < 0.05$ (cluster-forming threshold at voxel level: $P < 0.001$).

To identify task-related co-activation common to all clusters, we computed the overlap between the brain-wide co-activation patterns of all MACM-CBP-derived clusters using a minimum-statistic conjunction (Nichols et al. 2005).

Contrasts. To compare the brain-wide co-activation pattern between clusters, we first computed the voxel-wise differences between the ensuing ALE maps. Each of these difference scores was then compared with a null distribution. A full description of this procedure is provided in Supplementary Methods I.8. This test yielded a posterior probability *P* testing that the difference was not due to random noise in an exchangeable set of labels based on the proportion of lower differences in the random exchange. The resulting probability values were then thresholded at $P > 0.95$ (95% chance for true difference) and masked by the respective main effects, that is, the significant effects of the MACM for the minuend (e.g., the difference "Cluster A – Cluster B" was inclusively masked by the main effect of Cluster A).

Finally, we computed the specific co-activation pattern for all derived clusters, that is, brain regions significantly more co-activated with a given cluster than with any of the other clusters. This was achieved by performing a minimum-statistic conjunction across the results of the 4 contrasts between a given cluster and the remaining others.

RSFC for Each Cluster

RSFC analyses were performed on the normalized resting-state fMRI images as described at 2.2.3.1. and in Supplementary Methods I.7. These latter were first smoothed by a 5-mm full-width at half-maximum (FWHM) Gaussian kernel to improve signal-to-noise ratio and to compensate for residual anatomical variations.

Time series of the seed region were extracted for all gray matter voxels. The cluster time course was then expressed as the first eigenvariate of these voxels' time courses. Linear (Pearson) correlations between the time series of each seed region (cluster) and all other gray matter voxels were computed to quantify RSFC. These voxel-wise correlation coefficients were then transformed into Fisher's z-scores. These Fisher's z-scores were entered into a flexible factorial model to test for consistency across subjects, testing for the significance of the main effects of connectivity for each cluster as well as the differences between the clusters.

The CBP-derived clusters were used as seeds for the RSFC analyses. In correspondence with the MACM analyses described above and in line with previous studies (Clos et al. 2013), we first calculated RSFC shared by all MACM-CBP-derived clusters. This was achieved by computing a conjunction across the main effect of positive connectivity of all clusters. Second, we examined the specific co-activation pattern of each cluster. These patterns were obtained by performing a conjunction analysis, for each cluster, across the contrasts between the main effect of a given cluster and all other clusters. All analyses were thresholded at $P < 0.05$ (cluster FWE-corrected, cluster-forming threshold: $P < 0.001$).

Shared Task-Related and RSFC: Conjunction Across MACM and RSFC Results

For cross-validation, the results shared between both MACM and RSFC analyses were then examined for each cluster using a minimum-statistic conjunction. This procedure aimed to characterize the whole-brain connectivity pattern that is similar in resting state and in MACM (cf. Bzdok et al. 2013; Cieslik et al. 2013; Clos et al. 2013). We performed the conjunction between RSFC and MACM for 1) Common pattern for all clusters and 2) Specific pattern of each cluster (i.e., differences between clusters). For all these conjunction analyses, only cluster extend ≥10 voxels were further reported.

Functional Characterization of the MACM-CBP-Derived Clusters

Forward and Reverse Inference on BrainMap Meta-data

Functional characterization of the right PMd clusters revealed by MACM-CBP was performed using the "behavioral domain" (BD) and "paradigm class" (PC) meta-data of the included experiments as assigned in the BrainMap database (Laird et al. 2009). A description of the behavioral processes covered by the Brainmap paradigm class taxonomy may be found at http://brainmap.org/taxonomy/paradigms.html. BDs include the main categories "cognition, action, perception, emotion, interoception," as well as their respective subcategories. In turn, PCs categorize the

specific task employed. To characterize the individual functional profile of each cluster, we performed quantitative "forward inference" and "reverse inference" as has been done in previous parcellation studies (Bzdok et al. 2013; Cieslik et al. 2013; Clos et al. 2013). In the forward inference approach, a cluster's functional profile is assessed by identifying taxonomic labels for which the probability of finding activation in the respective cluster is significantly higher than finding activation for that label across the whole database by chance. Significance was determined using a binomial test ($P < 0.05$ corrected for multiple comparisons using Bonferroni's method; Clos et al. 2013; Rottschy et al. 2013). That is, we tested whether the conditional probability of activation in a particular region given a particular label [P(Activation|Task)] was higher than the baseline probability of activating this particular region [P(Activation)]. In the reverse inference approach, a cluster's functional profile was determined by identifying the most likely BDs and PCs given activation in a particular cluster, that is, the likelihood P(Task|Activation). This likelihood can be derived from P(Activation|Task) as well as P(Task) and P(Activation) using Bayes' rule. Significance (at $P < 0.05$, corrected for multiple comparisons) was then assessed by means of a χ^2 test. In sum, forward inference assessed the probability of activation given a behavioral label, whereas reverse inference assessed the probability of each behavioral label given an activation.

As done previously, we also performed contrast analyses between the different clusters' functional profiles. These contrasts were, in turn, constrained to those experiments in BrainMap activating either cluster. From this pool of experiments, the base rate is the a priori probability of any focus to lie in either of the 2 compared clusters given that it is located in any of them. Forward inference here compared the activation probabilities between the 2 clusters given a task compared with the a priori base rate. This was again achieved by means of a binomial test ($P < 0.05$, corrected for multiple comparisons). In the reverse inference approach, we compared the occurrence probabilities of the tasks given activation in 1 cluster (rather than in the other). This probability comparison was again achieved by means of a χ^2 test ($P < 0.05$, corrected for multiple comparisons).

Results

Cortical Parcellation Based on Connectivity Pattern

As our study aimed to distinguish functional subregions (i.e., clusters) in the right PMd, we first examined the most stable cluster solution obtained with CBP based on MACM across a wide range of k-solutions (from $k = 2$ to $k = 11$). We then investigated whether the topographical organization revealed by the ensuing solution could be supported by CBP based on other modalities. In particular, we performed PDT-CBP and RSFC-CBP, again evaluating different cluster solutions (in the vicinity of the $k = 5$ solution found for MACM) based on their inter-subject stability.

Cortical Parcellation Based on Co-activation Pattern (MACM-CBP)

The information, separation, and consistency criteria jointly identified the 5-cluster (5k) solution as the best among the 10 k-means clustering solutions. The splitting of the 5 clusters into functional space is illustrated in Supplementary Figure 3 and described in Supplementary Results II.1 while the resulting 5 clusters are illustrated in Figure 2A.

The rendering of the 5 clusters separately on coronal plans with the respective number of voxels and MNI coordinates of their respective center of gravity are illustrated in Supplementary Figure 3B. In addition, MNI coordinates of their borders are listed in Supplementary Results II.2, and the derived subregions in MNI volume space are available at http://anima.fz-juelich.de/studies/Genon_CBPrightPMd_2016. The location of the clusters highlights a rostro-caudal organization along the superior and middle frontal gyri. This organization includes a rostral cluster that lies anteriorly to the precentral gyrus; a central cluster that lies at the intersection of the precentral sulcus and the superior/middle frontal gyri; and a caudal cluster that is located at the posterior

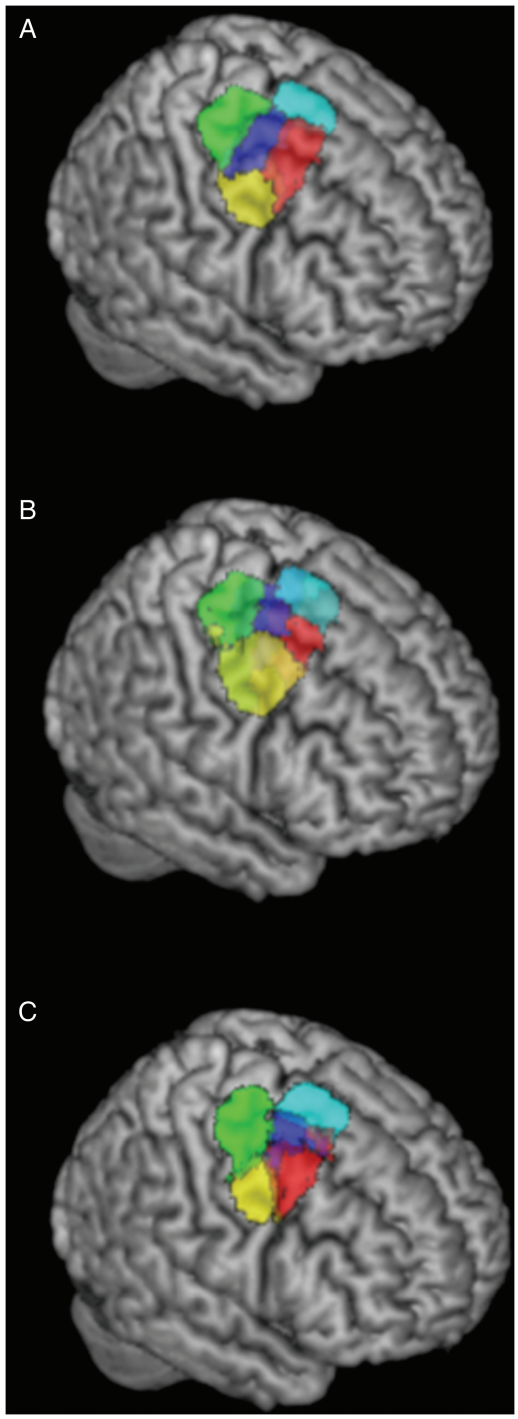

Figure 2. Rendering of the 5k solution yielded by different CBP modalities in the right PMd. (*A*) 5k solution yielded by MACM-CBP. (*B*) 5k solution yielded by PDT-CBP. (*C*) 5k solution yielded by RSFC-CBP.

part of the precentral gyrus. The location of the clusters further suggests a ventrodorsal organization with a ventral cluster adjacent to ventral PM and mainly overlapping with the precentral gyrus; the previously mentioned central cluster; and a dorsal cluster adjacent to inter-hemispheric premotor areas. For convenience, hereafter the clusters are labeled according to their anatomical location (i.e., rostral, caudal, central, ventral, and dorsal).

5-Cluster (5k) Solution Revealed by Structural Connectivity Pattern (PDT-CBP) and Unconstrained Functional Connectivity (RSFC-CBP)

The 5k solution identified by PDT-CBP showed good correspondence with the 5k solution identified by MACM-CBP with both rostro-caudal and ventrodorsal differentiation and a centrally located cluster (Fig. 2*B*).

The 5k solution yielded by RSFC-CBP is illustrated in Figure 2*C*. Matching MACM-CBP and PDT-CBP, it revealed a rostro-caudal organization and a ventrodorsal organization including and a centrally located cluster on the superior posterior frontal sulcus. We nevertheless note that the rostral and central border are less differentiated at the location of the superior frontal sulcus emphasizing that the rostro-caudal organization should be considered in term of gradient and not as spatially segregated subregions.

Examination of the stability of PDT-CBP-derived parcellation across resampling (half split) revealed that several k solutions show good stability. In particular, stability significantly increases (as reflected by both Cramer V and Normalized Mutual Information) from $k = 3$ to $k = 4$ and from this latter k solution to $k = 5$. In contrast, stability does not increase from $k = 5$ to $k = 6$ suggesting that we reach a local optimum at $k = 5$. Thus, the 5k solution is relatively well supported by DWI data. In contrast, examination of percentage of deviants and silhouette value across subjects indicated a general pattern of slightly linearly decrease of stability/consistency as k increases in RSFC-CBP. Nevertheless, examination of VI between subjects across k solutions showed that while VI tends to decrease from $k = 4$ to $k = 5$, it significantly increase from $k = 5$ to $k = 6$ suggesting that we also reach a local optimum at $k = 5$ with RSFC-CBP.

The overlap in term of number of voxels in the voxels between the 5k parcellation revealed by MACM-CBP and the 5k parcellation revealed by the 2 other CBP modalities is detailed in Supplementary Table 1 and described in Supplementary Results III.3.

Functional Connectivity of the Clusters Yielded by MACM-CBP

Common Functional Connectivity Patterns

The functional connectivity profile common to all clusters across both MACM and RSFC as well as functional connectivity profile common to all clusters only revealed by MACM are detailed in Table 1.

The results of the conjunction across the functional connectivity patterns of all 5 clusters across both MACM and RSFC analyses identified 2 regions common to all 5 clusters: postero-medial frontal cortex (SMA/pre-SMA) and the central cluster. That is, aside from common local connectivity with the central cluster, the postero-medial frontal cortex was the only brain region that showed consistent functional coupling with all identified clusters. Nevertheless, examination of the connectivity profile only observed by MACM additionally revealed that all clusters were co-activated with the bilateral IPS [Area hIP2/hIP3 (Choi et al. 2006)], the bilateral Area 44 (Amunts et al. 1999), the bilateral anterior insula, the bilateral prefrontal thalamus (Behrens et al. 2003), and the right pallidum. In contrast, RSFC revealed that all clusters were commonly coupled with the right rostral and ventral clusters and the primary somatosensory cortex [Area 2; (Grefkes et al. 2001)] extending to supramarginal gyrus [Area PFt (Casper et al. 2006, 2008)].

Cluster-Specific Functional Connectivity Patterns

Contrasting each cluster's functional connectivity patterns with those of all 4 other clusters identified each cluster's specific functional connectivity pattern. These findings are detailed in Table 1 and illustrated in Figure 3. For the sake of robustness of the highlighted functional connectivity profile, we mainly relied on the conjunction of unconstrained specific functional connectivity (as assessed with RSFC) and task functional connectivity (as assessed with MACM) as illustrated in Figure 3*C*. However, for the sake of completeness, we additionally examined the pattern yielded by MACM (Fig. 3*A*) and the pattern yielded by RSFC (Fig. 3*B*) separately. Nevertheless, the divergence between both approaches is discussed in Supplementary Discussion III.1.1.

Both approaches (RSFC and MACM) indicated specific connectivity of each cluster with a homotopic cluster in the left hemisphere. Each cluster showed additional specific connectivity profile reposted below.

Rostral Cluster. Both approaches showed that the rostral cluster was specifically connected to bilateral intraparietal sulcus [IPS: areas hIP1/hIP2 (Scheperjans et al. 2008)], lateral prefrontal cortex LPFC, midcingulate cortex and the right precuneus.

MACM further revealed that the rostral cluster was functionally coupled with the left ventral LPFC and the dorsomedial prefrontal cortex (DMPFC) while RSFC additionally revealed that it was functionally connected to the bilateral cerebellum lobule VII (Diedrichsen et al. 2009), the bilateral inferior temporal gyrus, the left precuneus, the right subiculum, and the right fusiform gyrus.

Caudal Cluster. Both approaches revealed that the caudal cluster was specifically connected to bilateral M1 [area 4p (Geyer et al. 1996)], bilateral SMA extending into midcingulate cortex, left cerebellum [lobule IV/V (Diedrichsen et al. 2009)], and right parietal operculum [areas OP1/OP3 (Eickhoff et al. 2006)] and frontal operculum.

MACM further revealed that the caudal cluster was functionally coupled with the posterior insula, the thalamus [premotor and prefrontal (Behrens et al 2003)], and the right putamen while RSFC additionally revealed functional connectivity of this cluster with parietal operculum subarea OP3/OP4 (Eickhoff et al. 2006).

Central Cluster. Both approaches showed that the central cluster was specifically connected to bilateral IPS (area hIP3) extending to superior parietal lobule [SPL: areas 7A/7PC/5l (Scheperjans et al. 2008)].

MACM further revealed that the central cluster was functionally coupled to the right fusiform gyrus [Area FG1/FG2 (Caspers et al. 2013)] and the left primary sensorimotor areas [Area 2 (Grefkes et al. 2001); Area 3b (Geyer et al. 1999)] while RSFC additionally revealed that it was functionally connected to left Broca's area [Area 44 (Amunts et al. 1999)], bilateral inferior parietal lobule [Area 2 (Grefkes et al. 2001); Area PFt & Area PFop; (Caspers et al. 2006, 2008)], and middle occipital gyrus.

Table 1 Common and specific functional connectivity of the 5 MACM-CBP-derived clusters across tasks (MACM) and rest (RSFC)

Region		Overlap with cytoarchitectonic area	x	y	z	Cluster size
Common to all clusters						
Tasks and rest						
Central cluster	R	NA	32	−3	57	107
Left PMd (central cluster's homotope)	L	NA	−33	−8	55	50
SMA/pre-SMA	L	NA	−8	5	51	58
	R	NA	5	8	49	13
	R	NA	6	4	64	10
Tasks only						
IPS	L	hIP3[i]	−34	−50	51	663
	R	hIP2/hIP3[d,i]	39	−47	50	189
Broca's area	R	Area 44[a]	54	9	28	305
	L	Area 44[a]	−53	6	31	256
Thalamus	R	Prefrontal thalamus[j]	12	−14	7	191
	L	Prefrontal thalamus[j]	−11	−16	7	171
Anterior insula	R	NA	36	23	1	165
	L	NA	−34	23	1	162
Basal ganglia	R	Pallidum/putamen	19	3	3	23
Rest only						
Rostral and ventral clusters	R	NA	26	−3	55	1369
Right somatosensory-cortex/supramarginal gyrus	R	Area 2[c]/Area PFt[l]	50	−32	48	301
Specific to rostral PMd						
Tasks and rest						
Left homotope	L	NA	−27	9	52	332
Middle frontal	L	NA	−40	29	33	166
Middle frontal	R	NA	30	8	42	1272[n]
			33	21	42	
			44	48	20	
			48	36	24	
		Fp1[b]	30	58	10	
MCC	R	NA	7	26	42	19
Inferior parietal/IPS	R	hIP1/hIP2[d]	42	−57	41	498
	L		−38	−58	41	389
Precuneus	R	NA	8	−62	50	63
Tasks only						
Inferior frontal gyrus	L	NA	−38	14	37	1071
	R	NA	32	29	−7	134
Rest only						
Inferior temporal gyrus	R	NA	62	−34	−18	601
	L		−57	−54	−15	160
Precuneus	L	NA	−6	−58	45	629
Cerebellum	L	Lobule VIIa[g]	−38	−65	−37	519
	R		34	−62	−33	100
Medial temporal lobe	R	Subiculum	29	−32	−18	318
Fusifurm gyrus	R	NA	−30	−40	−14	193
Specific to caudal PMd						
Tasks and rest						
Primary motor	R	Area 4p[e]	34	−26	60	1492[o]
Cortex	L	Area 4p[e]	−36	−29	60	535[o]
Left homotope						
SMA/Midcingulate cortex	R	NA	8	−10	50	153
	L		−5	−16	53	67
Cerebellum	L	Lobule VI/V[g]	−18	−57	−20	350
Parietal operculum	R	Area OP1/OP3[h]	47	−21	20	78
Frontal operculum	R	NA	44	−3	14	16
Tasks only						
Putamen	R	NA	31	−6	−1	66
Thalamus	R	Prefrontal/premotor thalamus [j]	14	−19	8	60
Posterior insula	R	NA	43	1	12	44
Rest only						
Parietal operculum	L	Area OP3/OP4[h]	−42	−21	18	366

Continued

Table 1 Continued

Region		Overlap with cytoarchitectonic area	x	y	z	Cluster size
Specific to central PMd						
Tasks and rest						
IPS/superior	R	Area 7A[i]/Area7PC[i]/hIP3[i]	26	−58	57	405
Parietal lobule	L	Area 7A[i]/Area 7PC[i]/Area 5l[i]	−28	−56	61	335
		Area 7A[i]	−19	−75	44	71
			−14	−67	58	33
Left homotope	L	NA	−25	−8	56	553
Tasks only						
Fusiform gyrus	R	Area FG1/FG2[k]	38	−68	−12	65
Somatosensori area	L	Area2[c]/Area 3b[e,f]	−38	−36	48	13
Rest only						
Inferior parietal lobule	R	Area2[c]/Area PFt[l]/Area PFop[l]	35	−41	48	1656
	L		−34	−44	47	1848
Middle occipital gyrus	L	NA	−23	−76	32	136
	R		29	−74	34	112
Broca area	L	Area 44[a]	−52	6	29	133
Specific to ventral PMd						
Tasks and rest						
Superior temporal	R	NA	59	−41	12	49
Left homotope	L	NA	−46	−4	48	356
Tasks only						
Visual cortex	R	hOc5[m]	50	−66	5	68
Rest only						
Inferior frontal	R	Area 45[a]	46	17	23	1277
Gyrus	L		−44	17	25	355
	R	NA	43	34	−7	259
Posterior middle	R	NA	60	−44	8	660
Temporal gyrus	L	NA	−58	−51	10	355
Specific to dorsal PMd						
Tasks and rest						
Left homotope	L	NA	−8	4	64	126
Inferior frontal gyrus/insula	R	NA	49	10	3	105
	L		−49	7	2	85
Putamen	R	NA	25	11	2	55
MCC	R	NA	10	10	40	22
Tasks only						
Broca's area	L	Area 44[a]	−52	10	3	505
	R	Area 44/45[a]	55	15	6	325
Rest only						
Middle frontal gyrus	R	NA	27	48	24	511
	L		−30	46	22	468
Anterior cingulate cortex	L	NA	−8	18	31	496
	R		9	20	30	462
Cerebellum	L	Lobule VIIa[g]	−42	−54	−33	139
Pre-SMA	R	NA	9	24	60	59

Note: NA, not assigned to any known probability map/not applicable.
[a]Amunts et al. (1999).
[b]Bludau et al. (in press).
[c]Grefkes et al. (2001).
[d]Choi et al. (2006).
[e]Geyer et al. (1996).
[f]Geyer et al. (1999).
[g]Diedrichsen et al. (2009).
[h]Eickhoff et al. (2006).
[i]Scheperjans et al. (2008).
[j]Behrens et al. (2003).
[k]Caspers et al. (2013).
[l]Caspers et al. (2006); Caspers et al. (2008).
[m]Malikovic et al. (2007).
[n]The region is part of the local connectivity of the rostral PMd itself (1083 voxels).
[o]The region is part of the local connectivity of the caudal PMd itself (1765 voxels) in the right hemisphere or its left-side homotope in the left hemisphere; CBP, Co-activation-based parcellation; MACM, meta-analytic connectivity modeling; RSFC, resting state functional connectivity; PMd, dorsal Premotor Cortex; IPS, intraparietal sulcus; SMA, supplementary motor area.

Ventral Cluster. Both approaches indicated that the ventral cluster was specifically connected to the right posterior superior temporal gyrus.

MACM further revealed that the ventral cluster was coactivated with right visual extrastriate cortex [hOC5 (Malikovic et al. 2007)] while RSFC showed that it was also connected to the bilateral posterior middle temporal gyrus and the bilateral ventral PFC [inferior frontal gyrus including Area 45 (Amunts et al. 1999)].

Dorsal Cluster. Both approaches indicated that the dorsal cluster was specifically connected to bilateral inferior frontal gyrus

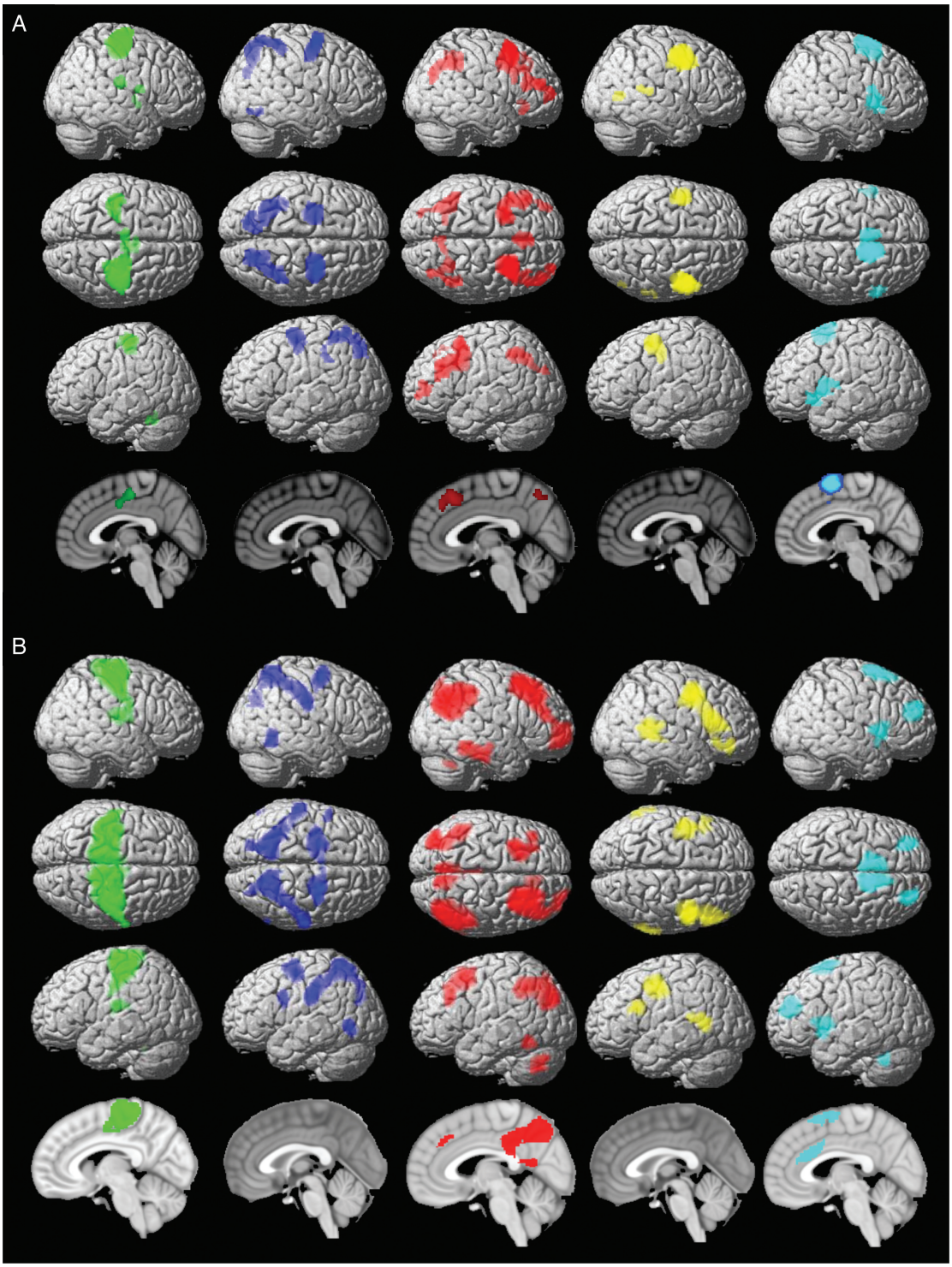

Figure 3. Specific functional connectivity profile of the MACM-CBP-derived subregions. Color code: green = caudal cluster, blue = central cluster, red = rostral cluster, yellow = ventral cluster, light blue = dorsal cluster. (*A*) Task functional connectivity (MACM). (*B*) RSFC (*C*) Conjunction of RSFC and MACM functional connectivity profile for each cluster.

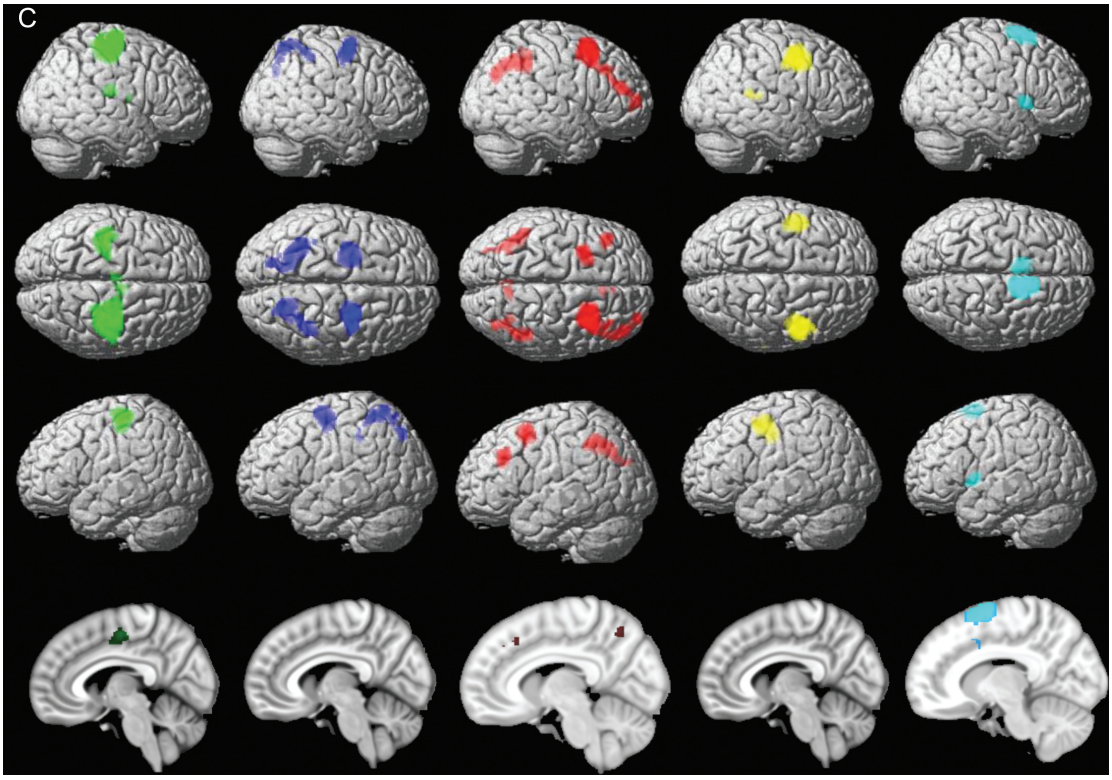

Figure 3. Continued.

slightly extending to the insula, the right putamen, and the right MCC.

MACM further revealed that the ventral cluster was coactivated with Broca's area [Area 44 (Amunts et al. 1999)] while RSFC revealed that it was functionally connected to middle frontal gyrus, bilateral ACC, left cerebellum [lobule VII, (Diedrichsen et al. 2009)], and right pre-SMA.

Functional Characterization of the Clusters Yielded by MACM-CBP

Forward and Reverse Inference on BrainMap Taxonomic Meta-data

Functional characterization of the 5 right PMd clusters was performed by forward and reverse inference on the taxonomic labels (BDs and PCs) provided by the BrainMap database (Laird et al. 2009). BDs and PCs significantly associated with each cluster across both forward and reverse inference are illustrated in Figure 5 and summarized in Figure 4. A description of the behavioral processes covered by the Brainmap paradigm class taxonomy may be found at http://brainmap.org/taxonomy/paradigms.html.

As shown in Figure 4A, some paradigms appeared to be related to several clusters across both forward and reverse inference. In particular, the central cluster showed a common paradigm profile with the caudal cluster regarding the PCs finger tapping and drawing. In addition, it showed a common paradigm profile with the rostral and ventral clusters regarding saccades and anti-saccades. Furthermore, the central and rostral clusters showed a common association with the PC "mental rotation." Finally, it shared visual distractor processing/visual attention with the ventral cluster.

Furthermore, there were several PCs specifically related to one particular cluster. In particular, cognitive paradigms such as the *n*-back task or the Wisconsin Card Sorting Test were specifically related to the rostral cluster. In contrast, paradigms targeting basic motor performance, such as finger flexion/extension or isometric force paradigms, were specifically related to the caudal cluster. Finally, imagined movements, sequence learning, and visual pursuit/tracking paradigms were specifically associated with the central cluster.

Synthesizing these findings, the functional characterization according to PCs thus revealed that the rostral cluster was mainly associated with paradigms engaging higher cognitive functions such as working memory. In contrast, the caudal cluster was mainly related to paradigms targeting motor functions. In turn, the ventral cluster was mainly associated with visual attention and eye movement paradigms, whereas the dorsal cluster was preferentially associated with paradigms engaging hand movements such as finger tapping. Finally, the central cluster showed a mixed pattern of associations including paradigms targeting motor functions, visual attention/eyes movements, and spatial cognition.

As illustrated in Figure 4B, the functional characterization according to BDs of the BrainMap database corroborated the above-described pattern emerging from the PC analysis and furthermore showed that while the central cluster was specifically associated with action imagination, the ventral cluster was specifically associated with vision.

The likelihood ratio and probabilities values associated to each significant behavioral label for each cluster are illustrated in Figure 5 while the results of the contrast analyses between the different clusters' functional profiles are illustrated in Figure S4. These results revealed a cognitive-motor gradient along the rostro-caudal axis. The rostral cluster was more related to higher cognitive functions than the central one, which was, in turn, more related to higher cognitive functions than the caudal one. For example, the rostral cluster was more related to working memory than the central one, but this latter was more associated

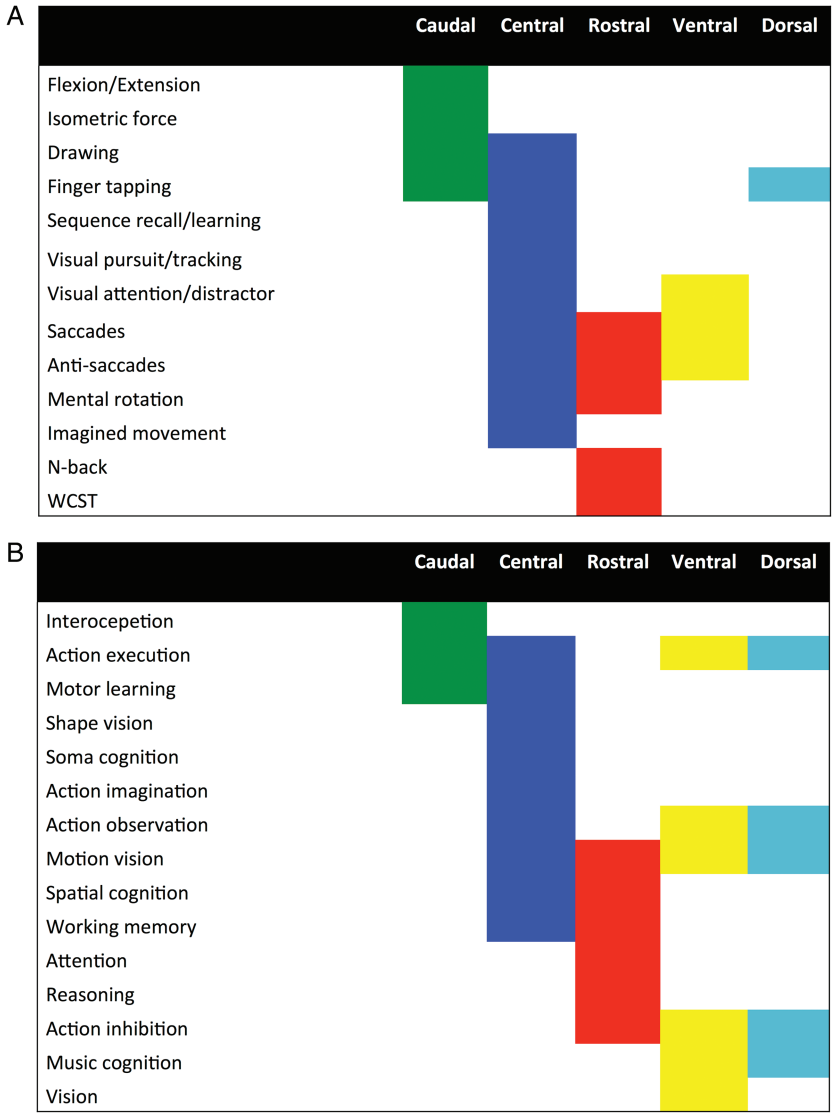

Figure 4. Summary of functional characterization of the clusters yielded by MACM-CBP as jointly reflected by forward and reverse inference. (*A*) Functional characterization according to the BrainMap paradigm classes. (*B*) Functional characterization according to the BrainMap behavioral domains.

with working memory than the caudal cluster. Motor functions showed the opposite pattern. For example, the caudal cluster was more associated with action execution than the central one, but this latter was more associated with action execution than the rostral cluster.

The contrast analyses furthermore highlighted that the ventral cluster showed the strongest association with eye movements/visual attention. Interestingly, the contrast analyses also showed that both the ventral and dorsal clusters were more related to speech functions than the rostral and the central ones. In addition, the dorsal cluster was more related to music cognition than the rostral and caudal clusters. However, the ventral and dorsal clusters differed in their functional profiles since the contrast between them revealed that while the ventral one was more associated with eye movements/visual attention, the dorsal one was more related to finger tapping.

Discussion

Using MACM-CBP, we found 5 distinct clusters within right PMd, which were corroborated by complementary structural and resting-state functional clustering approaches. Furthermore, by combining task-related (MACM) and task-free (RSFC) analyses, we characterized the whole-brain functional connectivity patterns of these 5 clusters. We finally used a meta-analytic approach to assign each of the 5 clusters a specific behavioral functional profile that complements the observed parcellation.

Consistent PMd Clustering Patterns Across Modalities

After testing a range of possible granularities based on co-activation patterns across studies (MACM), the 5-cluster (5k) solution was found to be optimally stable. It is noteworthy, however, that the choice of the cluster solution is an ill-posed problem (Eickhoff et al. 2015; Ryali et al. 2015), particularly since brain activity is likely characterized by multiple levels of organization (Bellec et al. 2015). While we focused here on one particular scale, consideration of other scales may well provide additional insight into the neurobiological organization of the right PMd.

The selected 5k solution consisted of 1) a rostral cluster adjacent to prefrontal cortex, 2) a central cluster at an intermediate location (and adjacent to all other ones), 3) a caudal cluster adjacent

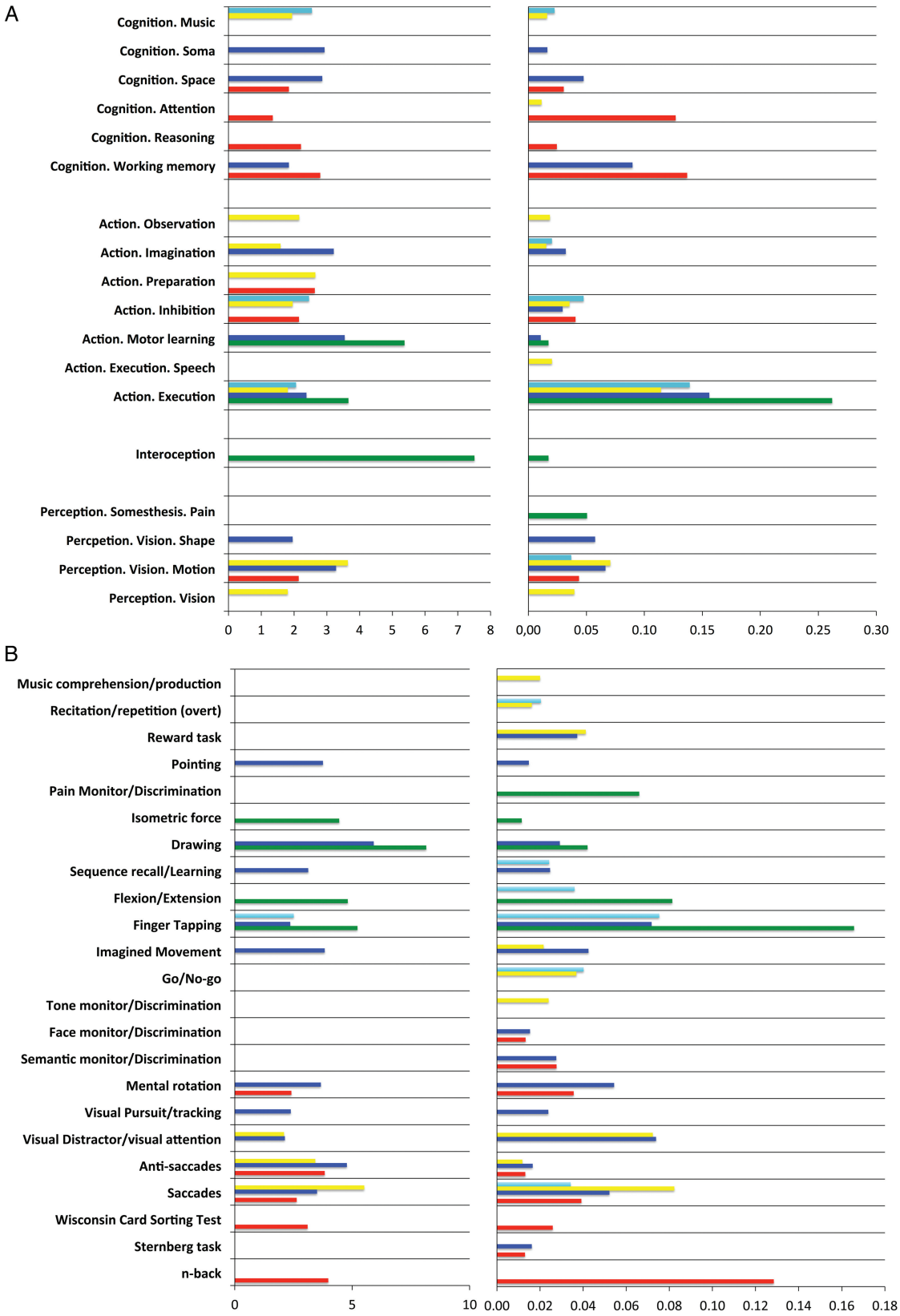

Figure 5. Functional decoding of the 5 right PMd clusters according to Brainmap. Functional decoding following forward inference expressed as likelihood ratio (left) and reverse inference expressed as probabilities (right). Color code: red, rostral; blue, central; green, caudal; yellow, ventral; light blue, dorsal. (*A*) Behavioral domains. (*B*) Paradigm classes.

to M1, 4) a ventral cluster adjacent to the PMv, and 5) a dorsal cluster bordering the medial premotor areas. This organization of the right PMd along both rostro-caudal and ventrodorsal axes was corroborated by additional parcellations based on structural connectivity (PDT) and unconstrained functional connectivity (RSFC). This cross-modal convergence suggests that the spatial organization of the right PMd revealed by MACM-CBP is robust across structural and functional criteria. It is important to highlight that the clusters' respective borders did not perfectly match across CBP modalities, suggesting that our methods have identified a topographical organization rather than a rigid set of borders. In particular, the rostro-caudal organization may be reflective of a gradient rather than sharply segregated subregions. Such a gradient mirrors the rostro-caudal organization suggested in nonhuman primates (see below) and corroborates at least one previous fMRI study in humans, in which it was associated with a cognitive-motor gradient (Orban et al. 2014).

Five Functional Subregions Within the Right PMd

Rostral PMd: Higher Cognitive Processes

Both the MACM and RSFC analyses revealed that the rostral PMd cluster was specifically functionally coupled with the midcingulate cortex, bilateral LPFC, and the IPS/inferior parietal regions. These regions are known to support higher cognitive functions such as executive functions (Collette et al. 2006), vigilant attention (Langner and Eickhoff 2013), and working memory (Rottschy et al. 2012). This cluster was also functionally connected with the precuneus, a region that is known to play a role in higher order visuospatial processes such as covert shift of attention and abstract mental imagery tasks (Cavanna and Trimble 2006). In line with this view, functional characterization across forward and reverse inference revealed that this cluster was engaged in functions such as working memory. In other words, the rostral cluster might be engaged in higher, potentially dynamic aspects of visuospatial imagery, which may possibly include short-term memory encoding of a location (Langner et al. 2014), maintenance of spatial information (including spatial rehearsal), and spatial updating. This cluster might also play a role in working memory even when the content is not overtly spatial (Nee et al. 2013).

The rostral cluster reported here bears similarity to area F7, the rostral subdivision of the PMd in nonhuman primates (Matelli et al. 1985, 1991). This region predominantly receives prefrontal inputs (Boussaoud et al. 1995; Rizzolatti and Luppino 2001) and contains neurons that are active when the animal engages cognitive functions such as spatial attention or memory (Boussaoud 2001; Lebedev and Wise 2001). In humans, a similar rostral PMd subregion, termed "pre-PMd," has been proposed, and connectivity between the pre-PMd and the prefrontal cortex has been suggested (Picard and Strick 2001). Similarly, previous functional studies have demonstrated that the most rostral part of the PMd (or pre-PMd) is frequently engaged in high-level cognitive operations (Hanakawa 2011), such as complex mental calculations (Zago et al. 2001). This evidence implies that our rostral cluster roughly corresponds to the proposed human pre-PMd and may be considered a potential homologue to F7 in the nonhuman primate. Of note, as there is currently no widely accepted landmark separating PM and prefrontal cortex, the rostral cluster found in the present study cannot be strictly considered a premotor region. In our study, the location of the rostral cluster, which is anterior to the precentral gyrus, leads us to consider it a transitional region in the ill-defined premotor-prefrontal dichotomy. Furthermore, its behavioral functional profile supports its consideration as a functional component of the prefrontal cortex, rather than a premotor module sensu-stricto.

Caudal PMd: Motor Functions

Task-based and RSFC analyses revealed that the most caudal PMd cluster is likely part of the brain's motor system, including bilateral M1, SMA, and the left cerebellum. The caudal cluster was also specifically functionally connected to right fronto-parietal operculum, which has been shown to support higher order somatosensory and sensorimotor processing (Eickhoff et al. 2010). Supporting this view, functional characterization of the caudal cluster revealed that it is engaged in action execution, motor learning, and interoception. It is thus likely that several functions that have frequently been assigned to the whole PMd are primarily subserved by this caudal subdivision. Such processes include 1) the creation of internal representations of action (or pragmatic body maps) which serve movement generation, understanding, and learning (Rizzolatti and Luppino 2001; Schubotz and von Cramon 2003), and 2) the organization of movement or action formulation (Schubotz and von Cramon 2003).

In line with our finding of a caudal cluster adjacent to M1 in humans, the posterior PMd adjacent to M1 in nonhuman primates has been defined as a distinct cytoarchitectonic and functional area. This caudal subregion, termed F2, is connected to M1 and the spinal cord (for reviews, see Geyer et al. 2000; Abe and Hanakawa 2009). The caudal PMd subregion has shown a similar connectivity pattern in humans, and fMRI studies have suggested that this subdivision (also referred to as the "PMd proper") is preferentially activated during movement preparation and execution (for a review, see Picard and Strick 2001). Such findings suggest a functional profile for the human caudal PMd which is similar to the one observed in nonhuman primates (Boussaoud 2001) and consistent with the one identified here for our caudal PMd cluster. Therefore, according to its integration into the sensorimotor network and its functional profile, characterized by processes related to motor preparation and programming, the caudal cluster may correspond to the nonhuman primate's caudal right PMd (area F2) and human right PMd proper.

Central PMd: the Core PMd

The central cluster was located between the rostral and caudal ones. Compared with all other clusters, it consistently showed a stronger functional coupling with the IPS and the SPL, regions that are known to be engaged in top-down/goal-driven modulatory processes (Corbetta and Shulman 2002). Considered separately, the MACM analysis further yielded connectivity with 2 different subregions of the ventral visual stream [respectively, FG2 and FDG1 (Caspers et al. 2015)]. Functional decoding revealed that the central cluster was related to both motor and cognitive functions (such as action execution and working memory), as well as to spatial cognition and motion perception. Together, these findings and the observation that all other clusters were functionally coupled with the central cluster suggest that the latter plays a core role within the right PMd mosaic by linking the functionally more specialized clusters within the right PMd.

Studies in nonhuman primates have also suggested a transitional region that lies at the border between F7 (i.e., rostral PMd) and F2 (i.e., caudal PMd), which has been named F2vr (for a review, see Abe and Hanakawa 2009). F2vr receives inputs from dorsolateral prefrontal cortex (DLPFC) and medial IPS (Luppino et al. 2003) and has been assumed to support the integration of a visuospatial parameter (target object) and a somatosensory/motor parameter (arm) to complete a motor plan (for a review,

see Abe and Hanakawa 2009). F2vr may thus subserve sensorimotor transformations. Our study provides support for the existence of a similar transitional cluster in humans within a central location, lying between the rostral "cognitive" cluster and the caudal "motor" one. Functional decoding showed that this subregion in human PMd is engaged in target and goal maintenance (working memory), visuospatial processes, action imagination, and action execution. This pattern suggests that our central cluster may, partly, include the human homologue of F2vr.

Ventral PMd: Eye-Related Functions

According to the functional decoding, the ventral and central PMd clusters shared several features. In particular, both were associated with saccades, anti-saccades, and visual attention paradigms. However, only the ventral cluster was significantly associated with the broader behavioral domain of vision. This behavioral profile fits with the specific co-activation of this latter cluster with the right visual cortex (see Supplementary Discussion III.2.1. for further discussion of task and rest functional connectivity of this cluster). These findings argue in favor of the ventral cluster being preferentially related to "eye-centered" functions. Such functions may cover learning sequences of eye movements, serial visual search, and visual attention. Nevertheless, the ventral cluster also showed broader associations, such as with action execution and action inhibition. Thus, while our ventral cluster may not strictly be considered an "eye field," it does likely overlap with the "premotor eye field" (see Supplementary Discussion III.2.2 for a description of the premotor eye field).

Dorsal PMd: Hand Preferences and Sequencing/Rhythm Aspects

In our MACM-CBP analysis, the dorsal PMd cluster was found to be closely coupled with the ventral cluster (see Supplementary Results II.1 and Supplementary Discussion III.1.2.). However, both PDT-CBP and RSFC-CBP clearly differentiated this dorsal subdivision as a separate cluster. Both MACM and RSFC identified specific functionally connectivity of this subdivision with bilateral prefrontal regions, insula, right putamen, and right MCC. These findings indicate that the dorsal cluster may be engaged in both motor and cognitive networks. Congruently, functional decoding showed a profile of associations that included motor, language, and music domains. Within the domain of motor functions, the dorsal cluster seemed to be preferentially related to hand/finger movements (i.e., finger tapping paradigms). In line with these findings, this part of the PMd was found to be activated for imitation of hand movements in a previous meta-analysis (Caspers et al. 2010). Our findings thus suggest that the dorsal cluster is related to both cognitive and motor processes, but appears to be particularly related to hand/finger movements, music, and language processing. There is evidence that music processing, language processing, and tapping might be related in certain respects (Overy et al. 2003); in particular, they may share sequencing and rhythm-processing aspects (Petkov et al. 2005; Flaugnacco et al. 2014). Therefore, although future studies are needed to more finely specify the motor and cognitive processes selectively engaging the dorsal cluster; for the time being, one can assume that this dorsal subregion preferentially supports sequencing and rhythm-processing aspects common to finger movements, music, and language.

Conclusion

Previous studies have suggested that the right PMd supports a wide range of motor and cognitive functions that may be topographically organized within this region, characterized by spatial gradients. Based on a quantitative data-driven approach, we showed that the right PMd can be robustly subdivided into 5 distinct functional modules. Our work highlighted a rostro-caudal organization with a rostral subregion supporting higher cognitive functions, a caudal subregion relatively more associated with motor functions, and a central subregion that may act as an interface between the rostral-cognitive and the caudal-motor subregions. Our study further revealed a ventrodorsal organization, including a ventral subregion that supports eye-field functions, a dorsal subregion that is preferentially related to hand/finger movements, and rhythm/sequencing aspects in cognitive and motor functions. How those modules may dynamically interact is discussed in Supplementary Discussion III.2.4. Finally, we suggest that the central subregion, positioned at the cross-roads of both gradients, plays an integrative role within this right PMd functional mosaic.

Supplementary Material

Supplementary material can be found at: http://www.cercor.oxfordjournals.org/.

Funding

The research leading to these results has received funding from the European Union Seventh Framework Programme (FP7/2007-2013) under grant agreement no. 604102 (Human Brain Project), the Deutsche Forschungsgemeinschaft (DFG, EI 816/4-1, EI 816/6-1, LA 3071/3-1), and the National Institute of Mental Health (R01-MH074457).

Notes

Furthermore, we thank Dr Matthew Glasser, Dr Saad Jbabdi, Dr Ricarda Schubotz, and Pr Alfred Anwander for helpful discussion and information. *Conflict of Interest*: None declared.

References

Abe M, Hanakawa T. 2009. Functional coupling underlying motor and cognitive functions of the dorsal premotor cortex. Behav Brain Res. 198:13–23.

Amft M, Bzdok D, Laird AR, Fox PT, Schilbach L, Eickhoff SB. 2015. Definition and characterization of an extended social-affective default network. Brain Struct Funct. 220:1031–1049.

Amiez C, Kostopoulos P, Champod A-S, Petrides M. 2006. Local morphology predicts functional organization of the dorsal premotor region in the human brain. J Neurosci. 26:2724–2731.

Amunts K, Schleicher A, Bürgel U, Mohlberg H, Uylings H, Zilles K. 1999. Broca's region revisited: cytoarchitecture and intersubject variability. J Compar Neurol. 412:319–341.

Behrens TEJ, Johansen-Berg H, Woolrich MW, Smith SM, Wheeler-Kingshott CAM, Boulby PA, Barker GJ, Sillery EL, Sheehan K, Ciccarelli O. 2003. Non-invasive mapping of connections between human thalamus and cortex using diffusion imaging. Nat Neurosci. 6:750–757.

Bellec P, Benhajali Y, Carbonell F, Dansereau C, Albouy G, Pelland M, Craddock C, Collignon O, Doyon J, Stip E, et al. 2015. Impact of the resolution of brain parcels on connectome-wide association studies in fMRI. NeuroImage. 123:212–228.

Boussaoud D. 2001. Attention versus intention in the primate premotor cortex. Neuroimage. 14:S40–S45.

Boussaoud D, di Pellegrino G, Wise SP. 1995. Frontal lobe mechanisms subserving vision-for-action versus vision-for-perception. Behav Brain Res. 72:1–15.

Brodmann K. 1909. Vergleichende Lokalisationslehre der Grosshirnrinde in ihren Prinzipien dargestellt auf Grund des Zellenbaues. Leipzig: Johann Ambrosius Barth.

Bzdok D, Langner R, Schilbach L, Jakobs O, Roski C, Caspers S, Laird AR, Fox PT, Zilles K, Eickhoff SB. 2013. Characterization of the temporo-parietal junction by combining data-driven parcellation, complementary connectivity analyses, and functional decoding. Neuroimage. 81:381–392.

Caspers J, Palomero-Gallagher N, Caspers S, Schleicher A, Amunts K, Zilles K. 2015. Receptor architecture of visual areas in the face and word-form recognition region of the posterior fusiform gyrus. Brain Struct Funct. 220:205–219.

Caspers J, Zilles K, Eickhoff SB, Schleicher A, Mohlberg H, Amunts K. 2013. Cytoarchitectonical analysis and probabilistic mapping of two extrastriate areas of the human posterior fusiform gyrus. Brain Struct Funct. 218:511–526.

Caspers S, Eickhoff SB, Geyer S, Scheperjans F, Mohlberg H, Zilles K, Amunts K. 2008. The human inferior parietal lobule in stereotaxic space. Brain Struct Funct. 212:481–495.

Caspers S, Geyer S, Schleicher A, Mohlberg H, Amunts K, Zilles K. 2006. The human inferior parietal cortex: cytoarchitectonic parcellation and interindividual variability. Neuroimage. 33:430–448.

Caspers S, Moebus S, Lux S, Pundt N, Schütz H, Mühleisen TW, Gras V, Eickhoff SB, Romanzetti S, Stöcker T. 2014. Studying variability in human brain aging in a population-based German cohort—rationale and design of 1000BRAINS. Front Aging Neurosci. 6:149.

Caspers S, Zilles K, Laird AR, Eickhoff SB. 2010. ALE meta-analysis of action observation and imitation in the human brain. Neuroimage. 50:1148–1167.

Cavanna AE, Trimble MR. 2006. The precuneus: a review of its functional anatomy and behavioural correlates. Brain. 129:564–583.

Choi EY, Yeo BT, Buckner RL. 2012. The organization of the human striatum estimated by intrinsic functional connectivity. J Neurophysiol. 108:2242–2263.

Choi HJ, Zilles K, Mohlberg H, Schleicher A, Fink GR, Armstrong E, Amunts K. 2006. Cytoarchitectonic identification and probabilistic mapping of two distinct areas within the anterior ventral bank of the human intraparietal sulcus. J Compar Neurol. 495:53–69.

Chouinard PA, Paus T. 2006. The primary motor and premotor areas of the human cerebral cortex. Neuroscientist. 12:143–152.

Cieslik EC, Zilles K, Caspers S, Roski C, Kellermann TS, Jakobs O, Langner R, Laird AR, Fox PT, Eickhoff SB. 2013. Is there "One" DLPFC in cognitive action control? Evidence for heterogeneity from co-activation-based parcellation. Cereb Cortex. 23: 2677–2689.

Clos M, Amunts K, Laird AR, Fox PT, Eickhoff SB. 2013. Tackling the multifunctional nature of Broca's region meta-analytically: co-activation-based parcellation of area 44. Neuroimage. 83:174–188.

Collette F, Hogge M, Salmon E, Van der Linden M. 2006. Exploration of the neural substrates of executive functioning by functional neuroimaging. Neuroscience. 139:209–221.

Corbetta M, Shulman GL. 2002. Control of goal-directed and stimulus-driven attention in the brain. Nat Rev Neurosci. 3:201–215.

Diedrichsen J, Balsters JH, Flavell J, Cussans E, Ramnani N. 2009. A probabilistic MR atlas of the human cerebellum. NeuroImage 46:39–46.

Eickhoff SB, Bzdok D, Laird AR, Kurth F, Fox PT. 2012. Activation likelihood estimation meta-analysis revisited. Neuroimage. 59:2349–2361.

Eickhoff SB, Bzdok D, Laird AR, Roski C, Caspers S, Zilles K, Fox PT. 2011. Co-activation patterns distinguish cortical modules, their connectivity and functional differentiation. Neuroimage. 57:938–949.

Eickhoff SB, Jbabdi S, Caspers S, Laird AR, Fox PT, Zilles K, Behrens TE. 2010. Anatomical and functional connectivity of cytoarchitectonic areas within the human parietal operculum. J Neurosci. 30:6409–6421.

Eickhoff SB, Schleicher A, Zilles K, Amunts K. 2006. The human parietal operculum. I. Cytoarchitectonic mapping of subdivisions. Cereb Cortex. 16:254–267.

Eickhoff SB, Stephan KE, Mohlberg H, Grefkes C, Fink GR, Amunts K, Zilles K. 2005. A new SPM toolbox for combining probabilistic cytoarchitectonic maps and functional imaging data. Neuroimage. 25:1325–1335.

Eickhoff SB, Thirion B, Varoquaux G, Bzdok D. 2015. Connectivity-based parcellation: critique and implications. Hum Brain Mapp. 36:4771–4792.

Flaugnacco E, Lopez L, Terribili C, Zoia S, Buda S, Tilli S, Monasta L, Montico M, Sila A, Ronfani L, et al. 2014. Rhythm perception and production predict reading abilities in developmental dyslexia. Front Hum Neurosci. 8:392.

Geyer S, Ledberg A, Schleicher A, Kinomura S, Schormann T, Bürgel U, Klingberg T, Larsson J, Zilles K, Roland PE. 1996. Two different areas within the primary motor cortex of man. Nature. 382:805–807.

Geyer S, Matelli M, Luppino G, Zilles K. 2000. Functional neuroanatomy of the primate isocortical motor system. Anat Embryol. 202:443–474.

Geyer S, Schleicher A, Zilles K. 1999. Areas 3a, 3b, and 1 of human primary somatosensory cortex. Neuroimage. 10:63–83.

Grefkes C, Geyer S, Schormann T, Roland P, Zilles K. 2001. Human somatosensory area 2: observer-independent cytoarchitectonic mapping, interindividual variability, and population map. Neuroimage. 14:617–631.

Grosbras MH, Beaton S, Eickhoff SB. 2012. Brain regions involved in human movement perception: a quantitative voxel-based meta-analysis. Hum Brain Mapp. 33:431–454.

Hanakawa T. 2011. Rostral premotor cortex as a gateway between motor and cognitive networks. Neurosci Res. 70: 144–154.

Hanakawa T, Honda M, Sawamoto N, Okada T, Yonekura Y, Fukuyama H, Shibasaki H. 2002. The role of rostral Brodmann area 6 in mental-operation tasks: an integrative neuroimaging approach. Cereb Cortex. 12:1157–1170.

Hardwick RM, Rottschy C, Miall RC, Eickhoff SB. 2013. A quantitative meta-analysis and review of motor learning in the human brain. Neuroimage. 67:283–297.

Hoshi E. 2013. Cortico-basal ganglia networks subserving goal-directed behavior mediated by conditional visuo-goal association. Front Neural Circuits. 7:158.

Hoshi E, Tanji J. 2007. Distinctions between dorsal and ventral premotor areas: anatomical connectivity and functional properties. Curr Opin Neurobiol. 17:234–242.

Johansen-Berg H, Behrens TEJ, Robson MD, Drobnjak I, Rushworth MFS, Brady JM, Smith SM, Higham DJ, Matthews PM. 2004. Changes in connectivity profiles define functionally distinct regions in human medial frontal cortex. Proc Natl Acad Sci USA. 101:13335–13340.

Kahnt T, Chang LJ, Park SQ, Heinzle J, Haynes J-D. 2012. Connectivity-based parcellation of the human orbitofrontal cortex. J Neurosci. 32:6240–6250.

Kantak SS, Stinear JW, Buch ER, Cohen LG. 2012. Rewiring the brain: potential role of the premotor cortex in motor control,

learning, and recovery of function following brain injury. Neurorehabil Neural Repair. 26:282–292.

Kelly C, Toro R, Di Martino A, Cox CL, Bellec P, Castellanos FX, Milham MP. 2012. A convergent functional architecture of the insula emerges across imaging modalities. Neuroimage. 61:1129–1142.

Kelly C, Uddin LQ, Shehzad Z, Margulies DS, Castellanos FX, Milham MP, Petrides M. 2010. Broca's region: linking human brain functional connectivity data and non-human primate tracing anatomy studies. Eur J Neurosci. 32:383–398.

Klein JC, Behrens TE, Robson MD, Mackay CE, Higham DJ, Johansen-Berg H. 2007. Connectivity-based parcellation of human cortex using diffusion MRI: establishing reproducibility, validity and observer independence in BA 44/45 and SMA/pre-SMA. Neuroimage. 34:204–211.

Laird AR, Eickhoff SB, Kurth F, Fox PM, Uecker AM, Turner JA, Robinson JL, Lancaster JL, Fox PT. 2009. ALE meta-analysis workflows via the brainmap database: progress towards a probabilistic functional brain atlas. Front Neuroinformat 3:23.

Langner R, Eickhoff SB. 2013. Sustaining attention to simple tasks: a meta-analytic review of the neural mechanisms of vigilant attention. Psychol Bull. 139:870–900.

Langner R, Sternkopf MA, Kellermann TS, Grefkes C, Kurth F, Schneider F, Zilles K, Eickhoff SB. 2014. Translating working memory into action: behavioral and neural evidence for using motor representations in encoding visuo-spatial sequences. Hum Brain Mapp. 35:3465–3484.

Lebedev MA, Wise SP. 2001. Tuning for the orientation of spatial attention in dorsal premotor cortex. Eur J Neurosci. 13:1002–1008.

Luppino G, Rozzi S, Calzavara R, Matelli M. 2003. Prefrontal and agranular cingulate projections to the dorsal premotor areas F2 and F7 in the macaque monkey. Eur J Neurosci. 17:559–578.

Malikovic A, Amunts K, Schleicher A, Mohlberg H, Eickhoff SB, Wilms M, Palomero-Gallagher N, Armstrong E, Zilles K. 2007. Cytoarchitectonic analysis of the human extrastriate cortex in the region of V5/MT+: a probabilistic, stereotaxic map of area hOc5. Cereb Cortex. 17:562–574.

Matelli M, Luppino G, Rizzolatti G. 1985. Patterns of cytochrome oxidase activity in the frontal agranular cortex of the macaque monkey. Behav Brain Res. 18:125–136.

Matelli M, Luppino G, Rizzolatti G. 1991. Architecture of superior and mesial area 6 and the adjacent cingulate cortex in the macaque monkey. J Compar Neurol. 311:445–462.

Mazziotta J, Toga A, Evans A, Fox P, Lancaster J, Zilles K, Woods R, Paus T, Simpson G, Pike B. 2001. A probabilistic atlas and reference system for the human brain: International Consortium for Brain Mapping (ICBM). Phil Trans R Soc Lond Ser B Biol Sci. 356:1293–1322.

Nee DE, Brown JW, Askren MK, Berman MG, Demiralp E, Krawitz A, Jonides J. 2013. A meta-analysis of executive components of working memory. Cereb Cortex. 23:264–282.

Nichols T, Brett M, Andersson J, Wager T, Poline J-B. 2005. Valid conjunction inference with the minimum statistic. Neuroimage. 25:653–660.

Nickl-Jockschat T, Rottschy C, Thommes J, Schneider F, Laird AR, Fox PT, Eickhoff SB. 2015. Neural networks related to dysfunctional face processing in autism spectrum disorder. Brain Struct Funct. 220:2355–2371.

Orban P, Doyon J, Petrides M, Mennes M, Hoge R, Bellec P. 2014. The richness of task-evoked hemodynamic responses defines a pseudohierarchy of functionally meaningful brain networks. Cereb Cortex. 25:2658–2669.

Overy K, Nicolson RI, Fawcett AJ, Clarke EF. 2003. Dyslexia and music: measuring musical timing skills. Dyslexia. 9:18–36.

Petkov CI, O'Connor KN, Benmoshe G, Baynes K, Sutter ML. 2005. Auditory perceptual grouping and attention in dyslexia. Cogn Brain Res. 24:343–354.

Picard N, Strick PL. 2001. Imaging the premotor areas. Curr Opin Neurobiol. 11:663–672.

Rizzolatti G, Luppino G. 2001. The cortical motor system. Neuron. 31:889–901.

Rizzolatti G, Luppino G, Matelli M. 1998. The organization of the cortical motor system: new concepts. Electroencephalogr Clin Neurophysiol. 106:283–296.

Rottschy C, Caspers S, Roski C, Reetz K, Dogan I, Schulz JB, Zilles K, Laird AR, Fox PT, Eickhoff SB. 2013. Differentiated parietal connectivity of frontal regions for "what" and "where" memory. Brain Struct Funct. 218:1551–1567.

Rottschy C, Langner R, Dogan I, Reetz K, Laird AR, Schulz JB, Fox PT, Eickhoff SB. 2012. Modelling neural correlates of working memory: a coordinate-based meta-analysis. Neuroimage. 60:830–846.

Ryali S, Chen T, Padmanabhan A, Cai W, Menon V. 2015. Development and validation of consensus clustering-based framework for brain segmentation using resting fMRI. J Neurosci Methods. 240:128–140.

Scheperjans F, Eickhoff SB, Homke L, Mohlberg H, Hermann K, Amunts K, Zilles K. 2008. Probabilistic maps, morphometry, and variability of cytoarchitectonic areas in the human superior parietal cortex. Cereb Cortex 18:2141–2157.

Schubotz RI, Anwander A, Knösche TR, von Cramon DY, Tittgemeyer M. 2010. Anatomical and functional parcellation of the human lateral premotor cortex. Neuroimage. 50: 396–408.

Schubotz RI, von Cramon DY. 2003. Functional–anatomical concepts of human premotor cortex: evidence from fMRI and PET studies. Neuroimage. 20:S120–S131.

Smith EE, Jonides J. 1999. Storage and executive processes in the frontal lobes. Science. 283:1657–1661.

Tomassini V, Jbabdi S, Klein JC, Behrens TEJ, Pozzilli C, Matthews PM, Rushworth MFS, Johansen-Berg H. 2007. Diffusion-weighted imaging tractography-based parcellation of the human lateral premotor cortex identifies dorsal and ventral subregions with anatomical and functional specializations. J Neurosci. 27:10259–10269.

Wang J, Yang Y, Fan L, Xu J, Li C, Liu Y, Fox PT, Eickhoff SB, Yu C, Jiang T. 2015. Convergent functional architecture of the superior parietal lobule unraveled with multimodal neuroimaging approaches. Hum Brain Mapp. 36:238–257.

Wise SP. 1985. The primate premotor cortex: past, present, and preparatory. Annu Rev Neurosci. 8:1–19.

Yeo BTT, Krienen FM, Sepulcre J, Sabuncu MR, Lashkari D, Hollinshead M, Roffman JL, Smoller JW, Zöllei L, Polimeni JR. 2011. The organization of the human cerebral cortex estimated by intrinsic functional connectivity. J Neurophysiol. 106:1125–1165.

Zago L, Pesenti M, Mellet E, Crivello F, Mazoyer B, Tzourio-Mazoyer N. 2001. Neural correlates of simple and complex mental calculation. Neuroimage. 13:314–327.